STScI | SPACE TELESCOPE SCIENCE INSTITUTE

Instrument Science Report ACS ISR 2018-05

Updates to the CALACS Cosmic Ray Rejection Routine: ACSREJ

N. D. Miles, P. L. Lim, A. Bellini, and N. A. Grogin

September 28, 2018

Abstract

This report presents an analysis of the updated version of the `ACSREJ` *contained in the current release of* `hstcal` *and available for download via AstroConda. The updated* `ACSREJ` *algorithm remedies a bug that caused the* `ERR` *extensions to be underestimated by a factor of* $1/\sqrt{g}$*, where* g *is the CCD gain. This fix triggered a reprocessing of all ACS/WFC superdarks and consequentially affects all ACS/WFC observations. The effect of the increased error contributed from the superdarks is most pronounced for observations with extremely low background* ($\leq 2e^{-}$)*. Typical backgrounds in ACS/WFC observations are well above this limit and so for most cases the total noise is still dominated by the amplifier read noise and the sky background. Next, the core algorithm has been updated to use the* `ERR` *extensions when performing statistical rejection of cosmic rays, as opposed to an estimate derived from the comparison image. The updates to the rejection algorithm required modifications to be made to the cosmic ray rejection table,* `CRREJTAB`*. These updates only affect CR-SPLIT observations and a photometric analysis concludes the changes have no affect on actual sources. Lastly, in order to make the effects of* ***newbias*** *keyword more explicit, it was changed to be* ***readnoise_only****. This keyword is only used to combine images with* $EXPTIME = 0$ *(i.e. bias frames) and as such only affects the generation of the ACS/WFC superbias reference files.*

1 Introduction

Ever since the discovery of cosmic rays by Victor Hess in 1912 (Hörandel 2013), cosmic rays have been under constant scrutiny by the scientific community. They serve as probes

of fundamental physics and are produced in nature's most powerful accelerators in extreme environments, but for most observational astronomers they are of little scientific interest. Prior to the installation of the Advanced Camera for Surveys (ACS) on Hubble Space Telescope (HST), a robust algorithm to flag and remove cosmic rays from CR-SPLIT images taken with either of the CCD imaging channels on ACS was developed and tested (Mutchler et al. 1999). The core of the `ACSREJ` algorithm used to reject cosmic rays from CR-SPLIT images has remained largely unchanged since its inception, until now.

The newest version of `CALACS` at the time of this writing is v10.0.0. It is contained within the `hstcal` package, v2.0.0, that is bundled in the HST Data Processing (HSTDP) 2018.1 release. In section 2, an in-depth review of the cosmic ray rejection algorithm implemented in `ACSREJ` is provided. In section 3, the updates made to `ACSREJ` in `CALACS` v10.0.0 and the steps taken to validate these changes are elucidated. In section 4, the effects of these updates on ACS/WFC reference files are presented. Lastly, in section 5, the impacts on users are evaluated and recommendations are made on the basis of those impacts.

2 ACSREJ Algorithm Review

The `ACSREJ` algorithm was ported from the successful and robust cosmic ray rejection routine developed to combine WFPC observations and later on STIS and WFPC2 observations (Shaw et al. 1998). The algorithm looks for statistically significant deviations in a pixel's signal across a list of input images to determine in which images the pixel was affected by a cosmic ray. The rejection criterion for each pixel is computed using a mix of parameters derived using all the input images, a single input image, and the cosmic ray rejection parameter table, `CRREJTAB` (Table 1).

Table 1: `CRREJTAB` parameters as defined in the ACS Data Handbook (Lucas et al. 2016)

Parameter	Default Value	Description
CRSPLIT	-	Number of exposures in CR-SPLIT
MEANEXP	INDEF	Average exposure time (in sec.) for CR-SPLIT images
SCALENSE	30	Multiplicative term (in percent) for the noise model.
INITGUES	minimum	Method for computing the initial-guess of the comparison image (minimum, median)
SKYSUB	mode	Sky fitting algorithm (mode, none)
CRSIGMAS	6.5, 5.5, 4.5	Rejection thresholds in sigma for consecutive iterations
CRRADIUS	2.1	Radius (in pixels) for propagating cosmic ray
CRTHRESH	0.5555	Propagation Factor
BADINPDQ	39	Data quality file bits to reject
CRMASK	yes	Flag CR-rejected pixels in input files?
CCDCHIP	-	CCD chip number (1 or 2)

2.1 Cosmic Ray Identification

The first step is to compute and subtract the sky background for each input image. The SKYSUB parameter controls how the background is computed and it only supports two values, mode and none. When SKYSUB is set to mode, the background to be subtracted is computed using the mode of each image. When SKYSUB is set to none, background subtraction is skipped. The second step is to generate the initial guess of the comparison image which serves as an approximation of the final cosmic-ray cleaned image. The comparison image can be created in one of two ways as specified by the INITGUES parameter. If INITGUES is set to minimum, then the comparison image is created by taking the minimum value of a single pixel across the entire list of input images. If INITGUES is set to median, then the comparison image is created by taking the median value.

To characterize the statistical deviation of a pixel from its nominal behavior the two scalar values defined below, $\Delta_n(x,y)$ and $\tau_n(x,y)$, are computed. If $\Delta_n(x,y) > \tau_n(x,y)$ then the pixel at (x,y) will be marked as a cosmic ray.

$$\Delta_n(x,y) = \frac{[p_n(x,y) - (sky_n + p(x,y))]^2}{T_n^2} \tag{1}$$

$$\tau_n(x,y) = \left(\frac{\sigma^2}{T_n^2}\right)[\sigma_{RN}^2 + \sigma_p^2(x,y) + \lambda(p(x,y) - sky_n)^2] \tag{2}$$

Definitions:

- $p_n(x,y)$:= signal at (x,y) in the nth image $[e^-]$
- sky_n := estimated sky background in the nth image $[e^-]$
- $T_n := \begin{cases} \text{EXPTIME}[s] & \text{if EXPTIME} > 0 \\ 1[s] & \text{otherwise} \end{cases}$
- $p(x,y)$:= signal at (x,y) in the comparison image $[e^-]$
- $\sigma_p(x,y)$:= poisson noise at (x,y) in the comparison image $[e^-]$
- σ_{RN} := read noise of amplifier used to read out (x,y) $[e^-]$
- σ := CRSIGMAS or CRTHRESH from CRREJTAB [dimensionless]
- λ := SCALENSE from CRREJTAB [dimensionless]

The first value, Δ_n, is a measure of the variance of the pixel in the nth image with respect to the comparison image plus the sky background from the nth image. The second value, τ_n, is a measure of the total variance expected from the contributing noise sources for a given pixel. The last term in τ_n, $\lambda(p(x,y) - sky_n)^2$, accounts for slight offsets in the pointing of HST between CR-SPLIT images. The PSF of the ACS/WFC is undersampled, so if the pointing of telescope is offset by a fraction of a pixel between two CR-SPLIT images, real sources (stars or galaxies) will be incorrectly rejected as cosmic rays. Whenever $\Delta_n(x,y) > \tau_n(x,y)$, in addition to the pixel at (x,y) being marked as a cosmic ray the

adjacent pixels within a radius of CRRADIUS will be marked as "spill" pixels. For these "spill" pixels, the same criterion for rejection is used with the exception that σ is now set to CRTHRESH, instead of CRSIGMAS, when computing $\tau_n(x, y)$. If multiple values are provided for CRSIGMAS, the process is iterated for each value with the comparison image being updated after each iteration.

2.2 Creating the Cosmic Ray Cleaned Image

Once the entire list of images has been analyzed, the next step is to combine all the values for a given pixel location (x, y) from each individual observation into a single value, p_{out}. For each pixel, the values are combined according to the summation in Eq 3 with the two new parameters, T and $m_n(x, y)$, defined below. The output pixel is in units of *electrons* and it represents the total contribution from every pixel in all the images where (x,y) is unaffected by cosmic rays. Effectively, it is the equivalent of a single image with an exposure time of T where signal deposited by cosmic rays has been replaced with the expected contributions from the *sky*.

$$p_{out}(x,y) = T\frac{\sum_{n=1}^{N}(p_n(x,y) - sky_n)m_n(x,y)}{\sum_{n=1}^{N} T_n m_n(x,y)} + \sum_{n=1}^{N} sky_n \tag{3}$$

Definitions:

- $T := \sum_{n=1}^{N} T_n$
- $m_n(x,y) := \begin{cases} 0 & \text{if } (x,y) \text{ is contaminated by a cosmic ray} \\ 1 & \text{otherwise} \end{cases}$

3 Updates to ACSREJ

3.1 Uncertainties

In versions of CALACS prior to the current release, v10.0.0, the formula for calculating the uncertainty had an erroneous factor of $1/\sqrt{g}$, where g is the gain of the amplifier used to read out a given pixel. Prior to Servicing Mission 4 (SM4), the possible gain settings for the HRC and WFC were 1.0, 2.0, 4.0, and 8.0 e^-/DN meaning the uncertainties could be underestimated by as much as $1/2\sqrt{2}$. Post-SM4, the possible gain settings for the WFC are 0.5, 1.0, 1.4, and 2.0 e^-/DN meaning the uncertainties could be overestimated by a factor of $\sqrt{2}$ or underestimated by a of factor $1/\sqrt{2}$.

The most straightforward way to confirm these updates is to analyze dark calibration frames taken with GAIN=2.0 e^-/DN. A bias-corrected dark frame has three main sources of noise: read noise, readout dark noise from the subtraction of the bias frame, and poisson noise from statistical fluctuations in the dark current accumulation. This allows for an easy verification of the removal of the erroneous factor of $1/\sqrt{g}$ on a per pixel basis. Since p_{out} represents the total signal from the N input images, its value must be normalized by N to yield the average signal expected in a single frame with an exposure time equal to one of

the individual exposures. This holds true for the computed uncertainty as well, so the total error must also be normalized by the number of images combined during the CR rejection process.

For a pixel, p, at (x, y) in the normalized output image, the final error is the quadrature sum of the contributing noise sources divided by $\sqrt{N}$, where the $1/\sqrt{N}$ factor signifies the improvement in the accuracy of the measurement of the pixel's true value due to the number of images included in the calculation.

$$\sigma = \frac{1}{\sqrt{N}} \sqrt{\sigma_{RN}^2 + \sigma_{bias}^2 + p(x_i, y_i)} \tag{4}$$

An anneal of darks taken as part of the CCD Daily Monitor routine calibration program was processed and combined to produce a CR-rejected image using two separate versions of `CALACS`, v9.2.0 and v10.0.0. For each of the two CR rejected images, the signal and error values are read in from the normalized `SCI` and `ERR` extensions, respectively. The predicted error is then computed using the `SCI` extensions according to Eq. 4 and compared to the values in the `ERR` extension. In Figure 1, the predicted error and final error computed by `CALACS` are compared for the two different versions. For clarity, the predicted error for `CALACS` v9.2.0 has been multiplied by $1/\sqrt{g}$ to demonstrate the effects of the bug. The agreement between the predicted error and the final error is apparent for both versions, but for v10.0.0 it is clear that the true error is properly estimated and the factor of $1/\sqrt{g}$ has been removed.

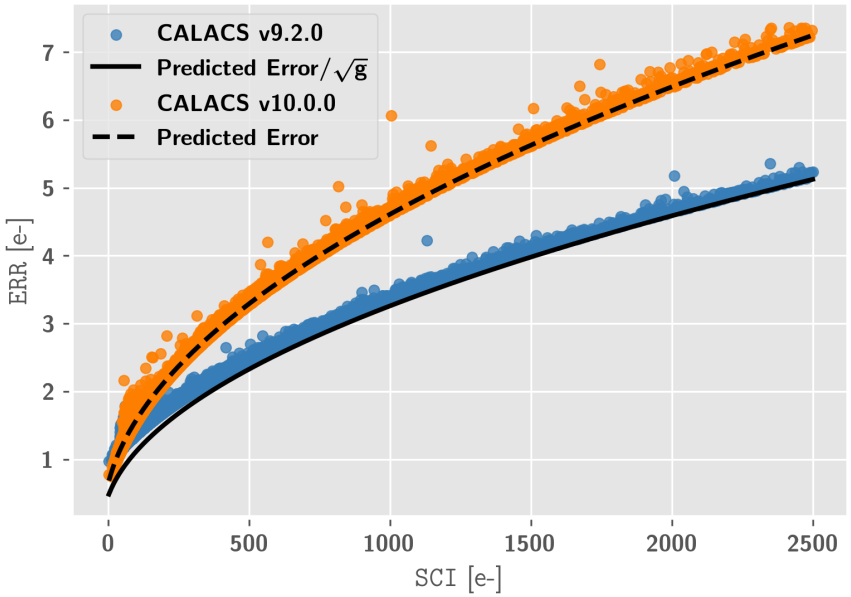

Figure 1: Comparison of the propagated uncertainties for the two CR-rejected images produced by the two versions of `CALACS`. There were a total of 48 images in this anneal cycle and so the noise on each measurement was reduced by $\sqrt{N} = \sqrt{48}$. For a list of the observations see Table 4 at the end of this report.

3.2 Thresholding Criterion

The noise model (Eq. 2) used for statistical rejection previously relied on the comparison image to estimate the variance for a given pixel as $\sigma_R^2 + \sigma_p^2(x, y)$. In `CALACS` v10.0.0 and

higher, this estimate has been replaced with the value contained in the ERR extension for the given pixel and so Eq. 2 becomes:

$$\tau_n(x,y) = \left(\frac{\sigma^2}{T_n^2}\right)[\sigma_{p_n}^2(x,y) + \lambda(p(x,y) - sky_n)^2] \tag{5}$$

The reason for this change is to correctly include noise contributions from readout dark when computing τ_n, which were previously unaccounted for. Readout dark was first quantified in ACS ISR 2014-02 (Coe et al. 2014) and again in ACS ISR 2017-13 (Ryon et al. 2017). Ryon et al. 2017 developed a robust method for computing the contributions to the overall noise from readout dark and these contributions are now included in all ACS/WFC superbiases. With these updates to the ACS/WFC superbiases, the changes to the ACSREJ noise model allow the noise contributions from readout dark to be accounted for.

In CALACS, cosmic ray rejection occurs immediately after the bias and CTE correction have been applied. The reason for this is that each subsequent correction (e.g. FLASHCORR, DARKCORR) adds additional noise which can have a deleterious effect on identifying cosmic rays that deposit a small number of electrons. The ERR extensions are initialized at the end of the bias correction step by summing in quadrature the poisson error, the read noise, and the value from the ERR extension of the relevant superbias after it has been multiplied by the gain (Chapter 3.4.1, Lucas et al. 2016). Hence, for any pixel affected by a cosmic ray its total noise will include a poisson term for the electrons deposited by the cosmic ray. The impact of these changes made to the noise model will necessitate a reduction of the σ parameter (CRSIGMAS) in Table 1) to compensate for the higher noise because $\sigma_{p_n}(x,y) > \sigma_p(x,y)$ whenever (x,y) is affected by a cosmic ray. This effect is made clear in Figure 2 that compares two different CR rejected products (bottom row) made from the same two CR-SPLIT images (top row). An analog of Figure 2 made with CTE corrected products may be found at the end of the paper.

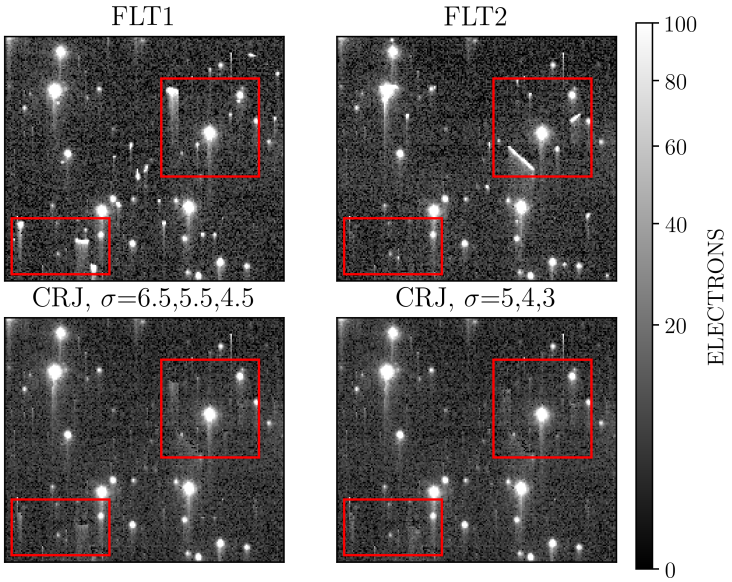

Figure 2: The effects of lowering the CRSIGMAS threshold when rejecting cosmic rays in CALACS v10.0.0. The greatest improvement comes in handling the CTE trails of cosmic rays, which is highlighted in the red boxes. If left behind, these trails could artificially raise background levels when performing local-sky subtraction using an annulus centered on the source.

To ensure that the lowering of the CRSIGMAS parameter does not have detrimental effects on actual sources, an analysis of 47 Tuc images observed as part of the CCD Stability Monitor program (Table 2) was performed. If the cosmic ray rejection parameters are too strict, then astrophysical sources could potentially have their central pixels flagged as cosmic rays resulting in false positives. Each pair of images with matching EXPTIME and APERTURE comprises a single CR-SPLIT association and so they are processed with CALACS to perform the bias correction, cosmic ray rejection, dark correction, and flat-field correction. This results in two FLT images and one CRJ image for each CR-SPLIT association.

PSF photometry is performed on the FLT images and the QFIT (Anderson et al. 2008) metric is used to threshold out all sources with poor fits (e.g. cosmic rays or blended sources). Sky-subtracted aperture photometry is performed on the CRJ images using a 10 pixel aperture and a sky annulus with an inner radius of 12 pixels and an outer radius of 16 pixels. The sources in CRJ images are analyzed via aperture photometry because of its increased sensitivity to the flagging of false positives compared to the fitting procedure utilized in PSF photometry. To determine if the relaxation is resulting in the misclassification of sources as cosmic rays, the residuals between the magnitudes from sources in the FLT images and their matching counterparts in the CRJ images are analyzed. For isolated sources, the residuals should be (< 0.1mag), however if this is not the case it would indicate that the cosmic ray rejection parameters are too strict.

FILENAME	EXPTIME	APERTURE
jd5702jmq_flt.fits	40.0	WFC1A-1K
jd5702jnq_flt.fits	40.0	WFC1A-1K
jd5702joq_flt.fits	40.0	WFC1B-1K
jd5702jpq_flt.fits	40.0	WFC1B-1K
jd5702jqq_flt.fits	40.0	WFC2C-1K
jd5702jrq_flt.fits	40.0	WFC2C-1K
jd5702jsq_flt.fits	40.0	WFC2D-1K
jd5702jtq_flt.fits	40.0	WFC2D-1K
jd5702k4q_flt.fits	40.0	WFC1A-512
jd5702k5q_flt.fits	40.0	WFC1A-512
jd5702k6q_flt.fits	40.0	WFC1B-512
jd5702k7q_flt.fits	40.0	WFC1B-512
jd5702k8q_flt.fits	40.0	WFC2C-512
jd5702k9q_flt.fits	40.0	WFC2C-512
jd5702kaq_flt.fits	40.0	WFC2D-512
jd5702kbq_flt.fits	40.0	WFC2D-512
jd5702kcq_flt.fits	40.0	WFC1B-2K
jd5702kdq_flt.fits	40.0	WFC1B-2K

Table 2: A subset of the data taken for the CCD Stability Monitor Program (proposal ID: 14511) used in the photometric evaluation.

In Figure 3, the residuals between the aperture and psf magnitudes is shown on the left, with a 500 by 500 pixel cutout of the corresponding CRJ image on the right. A subset of bright sources with excellent PSF fits was extracted by applying threshold cuts using the QFIT parameter and the magnitude. This subset was furthered partitioned according to the residuals between the aperture and PSF magnitudes as a means for easily identifying the cause of any outliers. Figure 3 demonstrates the perfect agreement between the magnitudes of bright and isolated stars measured on the FLT and on the CRJ images, proving that the lower CRSIGMAS parameter does not affect the shape of stellar sources.

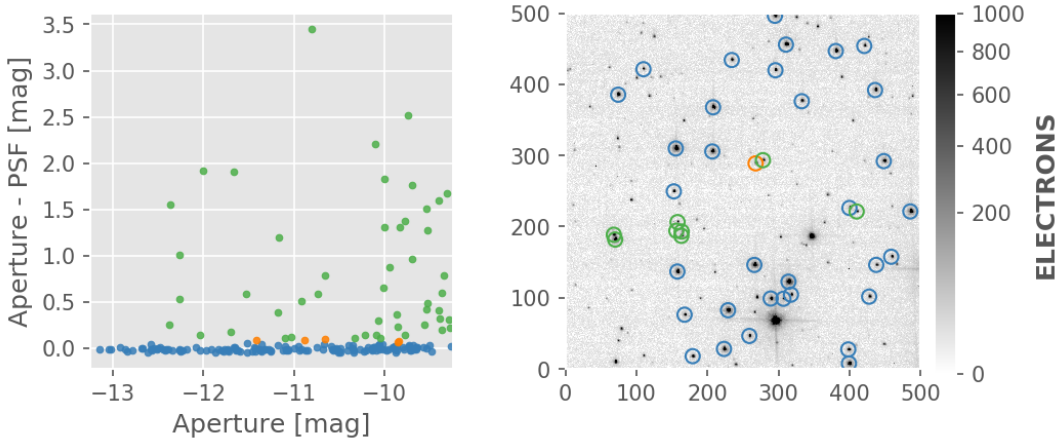

Figure 3: An example of the comparison between the instrumental aperture and psf magnitudes extracted from the CRJ and FLT, respectively. Blue identifies sources with residuals < 0.05, orange identifies sources with $0.05 \leq$ residuals ≤ 0.1, and green identifies sources with residuals ≥ 0.1. The image on the right is a small section of the CRJ shown here to highlight the types of sources corresponding to various thresholds. The two bright stars located at $(300, 50)$ and $(350, 190)$ suffered cosmic ray contamination in one of the two FLT exposures comprising the CR-SPLIT association. Hence, they were removed from the analysis of the FLT images by the QFIT cuts which is why they are not highlighted by a color aperture.

3.3 Parameter Changes

The ACSREJ algorithm command line argument, newbias, is used to handle the error propagation when combining bias frames. The argument ensures that only contributions from read noise are considered when computing the final error of the combined image and it is only used in the process of generating the superbiases. To make this more explicit, the argument was changed from newbias to readnoise_only. An example of the result of applying this argument may be seen in Figure 4. The leftmost image is the SCI extension, the middle image is the ERR extension generated by ACSREJ for the combined product, and the rightmost image is the same extension when the readnoise_only argument is passed. The difference, as expected, is that the poisson terms have been omitted when the readnoise_only argument is used.

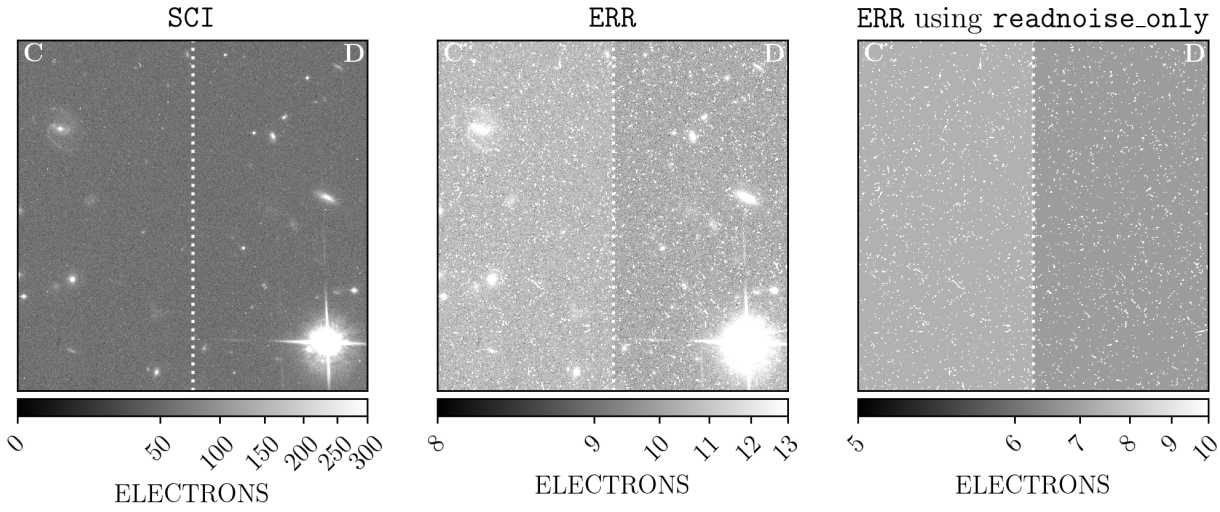

Figure 4: The white vertical line in each plot divides the chip into two quadrants according to amplifier used in the readout process. In each of the three plots the amplifiers used for each quadrant are labeled in the top left and top right corners. The two amplifiers, C and D, at the time this image was taken had read noises of $5.23e^-$ and $4.84e^-$, respectively. The pedestal offset between the two quadrants in the error arrays is due to differences in the read noise between the two amplifiers.

4 Updates to Reference Files

4.1 Superdarks

In light of the updates made to the error propagation, the ACS Team has reprocessed and redelivered all ACS/WFC superdarks. The newly generated superdarks will all have higher values stored in the `ERR` extensions, resulting in an increased noise contribution during the dark subtraction step of `CALACS`. This affects all data taken with the ACS/WFC where the gain does not equal 1 e^-/DN. As of August 1st, 2018 all files in the archive have been reprocessed with the newest set of reference files.

4.2 CRREJTAB

With the upgrades made to the noise model, the default values for the `CRSIGMAS` parameter are no longer optimal. The updated `CRREJTAB` has the default values of $5, 4, 3$ for the `CRSIGAMS` parameter. The new `CRREJTAB` was delivered to the INS Reference Data for Calibration and Tools (ReDCaT) Management Team for ingestion into the Calibration Reference Data System (CRDS). The new file, 29p1548cj_crr.fits, replaces the previous version, n4e12511j_crr.fits. All affected datasets will be reprocessed with this updated reference file after the release of HSTDP 2018.3.

5 Recommendations to Users

The HRC has been non-operational since SM4, so in the following sections the recommendations made assume that the observations are taken with the WFC and the default gain setting of 2 e^-/DN. When comparing data products generated with `CALACS` v9.2.0 and v10.0.0 the effects of these updates will be two-fold. Firstly, the error for every pixel in the `ERR` extension of a cosmic ray rejected product (i.e. CRJ or CRC) will increase by a factor of $\sqrt{g} \approx 1.4$. Secondly, the noise contributed by dark subtraction will have increased from v9.2.0 to v10.0.0.

The effects of the increased error in the `ERR` extensions will be minimal and only affect CR-SPLIT observations, but given advances in photometry packages they can be correctly accounted for. The commonly used photometry packages like `DAOPHOT` (Stetson 1987) or `DOLPHOT` (Dolphin 2016) typically compute the total noise for a given source directly from the `SCI` extensions and a user-supplied read noise; because of this their noise estimations will be unaffected by these increases. The more recently established `photutils` (Bradley et al. 2016) has functionality for supplying an error array when performing simple aperture photometry[1]. The uncertainty for the integrated flux of a given source is computed by summing in quadrature the value of all pixels contained within the aperture at the location of said source in the error array[2]. The `ERR` extensions contain all of the noise sources affecting a given pixel, that is, they contain the poisson terms from the source and sky, the calibration terms from processing with `CALACS`, and finally, the read noise. Thus, when performing simple aperture photometry it is recommended that users utilize this capability in `photutils` to correctly account for all sources of noise, regardless of the regime of operation (i.e. bright vs background limited sources).

Next, the increased noise from dark subtraction results from the updates made to the reference files and so it affects both CR-SPLIT and dithered observations. To analyze the effect of this increase, $\sigma_{total} = \sqrt{(g \times \sigma_{bias})^2 + (t \times \sigma_{dark})^2 + \sigma_R^2}$ is computed where σ_{dark} and σ_{bias} are the superdark and superbias `ERR` extensions, respectively, t is the exposure time of the observation, and σ_R is the read noise. The superdark and superbias used in this analysis are 27d1114fj_drk.fits and 27d11149j_bia.fits and both have a `USEAFTER` date of May 31st 2018 02:28:14. For each amplifier, the 3σ clipped mean of σ_{total} is computed and compared to just the read noise for the given amplifier. In Table 3, the difference between the sigma-clipped mean and the read noise is reported. The extra noise contributed by the updated reference files is at most 17.5% of the read noise value.

[1] https://photutils.readthedocs.io/en/stable/api/photutils.aperture_photometry.html
[2] https://photutils.readthedocs.io/en/stable/aperture.html#error-estimation

EXPTIME [s]	Amp A [e^-]	Amp B [e^-]	Amp C [e^-]	Amp D [e^-]
1	0.395	0.418	0.430	0.381
20	0.395	0.418	0.430	0.381
40	0.395	0.418	0.431	0.381
80	0.396	0.419	0.432	0.382
150	0.400	0.424	0.436	0.386
200	0.404	0.428	0.440	0.400
350	0.423	0.449	0.459	0.408
600	0.476	0.506	0.512	0.457
1000	0.614	0.655	0.649	0.587

Table 3: Additional noise imparted from bias and dark calibration.

The typical background for wide-band ACS/WFC observations with exposure times of several hundred seconds is several 10's of electrons (Sokol et al. 2012). For observations with narrow-band filters, the typical backgrounds range from 0.5 to 10 electrons (Sokol et al. 2012). However, because of the impacts of a low background on the pixel-based CTE correction (see Anderson et al. 2018 for the most recent characterization), users are advised to ensure that a background of at least $\sim$ 20 electrons is achieved in their observations. There are two ways to attain the desired background level: increase the exposure times or use post-flash capabilities (Miles 2018), with the caveat of additional noise from post-flash calibration. These options should be evaluated on the basis of the sources being studied.

For unresolved sources (e.g. unobscured stellar clusters) either option will suffice, but again it is important to understand there is additional noise added from the post-flash calibration step. For resolved objects, users should lengthen exposure times and avoid post-flashing at all cost. The detrimental effects on the morphological properties of resolved objects caused by the post-flash are irrecoverable. Hence, for background-limited sources it will likely be the case that the dominant noise sources are the read noise and the poisson noise from sky background and the source. However, if users choose to avoid post-flashing data and cannot raise the background level to the suggested $\sim$ 20 electrons, it is recommended that they include the noise contributions from the calibration steps applied to their data when computing the uncertainties on of their measurements.

Finally, when processing CR-SPLIT observations users should ensure that they are using the most recent version of the `CRREJTAB` reference file. Performing cosmic ray rejection with the previous version leads to residual cosmic ray contamination that is apparent in the combined image (see Figure 2). To ensure you have the most recent version please compare your filename to the one listed on the CRDS website[3].

[3] https://hst-crds.stsci.edu

6 Conclusion

The updates made to `ACSREJ` in `CALACS` v10.0.0 have led to several changes. The cosmic ray rejection parameter table, `CRREJTAB`, has been updated to compensate for the changes made to the noise model used in the cosmic ray rejection algorithm. A new version of this reference file was delivered and is ready for use with all data. A bug-fix has corrected the error propagation within `ACSREJ` leading to an increase in the noise for ACS/WFC superdarks taken with the default gain, as well as an increase in the noise for cosmic ray rejected products (CRJ or CRC) produced from CR-SPLIT observations. The impacts of these updates are greatest for faint sources in observations with an extremely low background ($\sim$ 0.5 electron), users working in this regime should take extra care in computing uncertainties for photometric measurements.

7 Acknowledgements

The authors would like to thank Michele De La Peña for helpful discussions on the background of the `newbias` keyword. The authors would like to also thank the following ACS Team members, in no particular order, for their contributions in improving the quality and readability of this ISR: Roberto Avila, Ralph Bohlin, Jenna Ryon, Nimish Hathi, and Marco Chiaberge.

References

Anderson, J. and J.E. Ryon (2018). *Improving the Pixel-Based CTE-correction Model for ACS/WFC*. ACS ISR 2018-04. Space Telescope Science Institute.

Anderson, J. et al. (2008). "Deep Advanced Camera for Surveys Imaging in the Globular Cluster NGC 6397: Reduction Methods". In: *Astronomical Journal* 135, pp. 2114–2128. DOI: 10.1088/0004-6256/135/6/2114. arXiv: 0803.0740 [astro-ph].

Bradley, L. et al. (2016). *astropy/photutils: v0.5*. DOI: 10.5281/zenodo.596036. URL: https://doi.org/10.5281/zenodo.596036.

Coe, D. and N.A. Grogin (2014). *Readout Dark: Dark Current Accumulation During ACS/WFC Readout*. ACS ISR. 2014-02: Space Telescope Science Institute.

Dolphin, A. (2016). "DOLPHOT: Stellar photometry". In: *Astrophysics Source Code Library*. ascl: 1608.013.

Hörandel, J. R. (2013). "Early cosmic-ray work published in German". In: *American Institute of Physics Conference Series*. Ed. by J. F. Ormes. Vol. 1516. American Institute of Physics Conference Series, pp. 52–60. DOI: 10.1063/1.4792540. arXiv: 1212.0706.

Lucas, R.A. et al. (2016). *ACS Data Handbook*. Vol. 8.0. Space Telescope Science Institute.

Miles, N.D. (2018). *Updates to Post-Flash Calibration for the Advanced Camera for Surveys Wide Field Channel*. ACS ISR 2018-03. Space Telescope Science Insitute.

Mutchler, M., W. Hack, R. Jedrzejewski, and D. Van Orsow (1999). *ACS Calibration Pipeline Testing: Cosmic Ray Rejection*. ACS ISR 1999-09. Space Telescope Science Insitute.

Ryon, J.E., N.A. Grogin, and D. Coe (2017). *Accounting for Readout Dark in ACS/WFC Superbiases*. ACS ISR 2017-13. Space Telescope Science Institute.

Shaw, D. and P. Hodge (1998). *Cosmic Ray Rejection in STIS CCD Images*. STIS ISR 1998-22. Space Telescope Science Insitute.

Sokol, J., J. Anderson, and L.J. Smith (2012). *Assessing ACS/WFC Sky Backgrounds*. ACS ISR 2012-04. Space Telescope Science Institute.

Stetson, P.B. (1987). "DAOPHOT - A computer program for crowded-field stellar photometry". In: *PASP* 99, pp. 191–22.

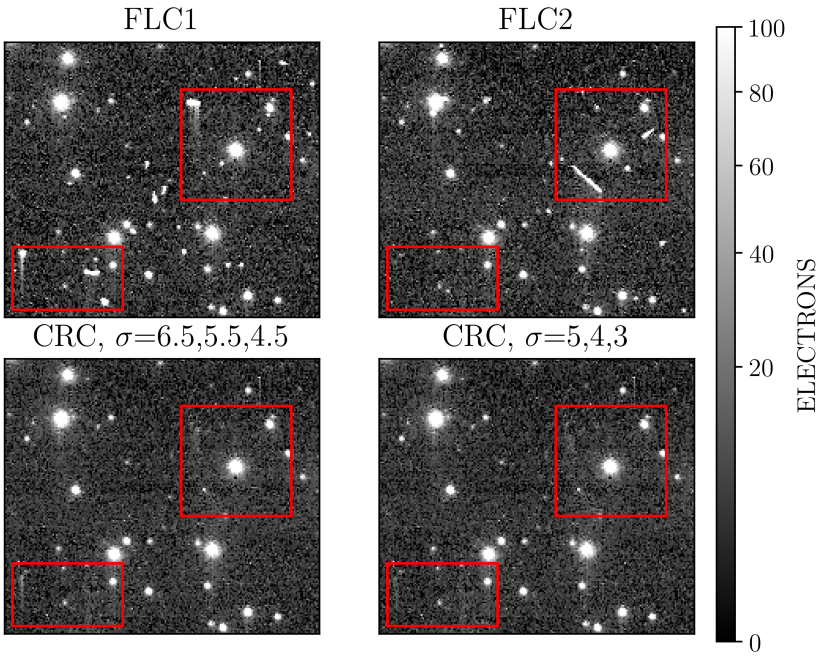

Figure 5: An example of the effects of lowering the `CRSIGMAS` threshold when rejecting cosmic rays in `CALACS` v10.0.0. This is the same as in Figure 2, but here the CTE-corrected products are used. Again, the red boxes highlight areas where the improvements are obvious.

FILENAME	EXPTIME	DATE-OBS	APERTURE	PROPOSID
jd4yfkldq_raw.fits	1000.5	2017-06-28	WFC	14517
jd4yflljq_raw.fits	1000.5	2017-06-28	WFC	14517
jd4yfmlpq_raw.fits	1000.5	2017-06-28	WFC	14517
jd4yfnltq_raw.fits	1000.5	2017-06-28	WFC	14517
jd4yfou0q_raw.fits	1000.5	2017-06-30	WFC	14517
jd4yfpudq_raw.fits	1000.5	2017-06-30	WFC	14517
jd4yfqv3q_raw.fits	1000.5	2017-06-30	WFC	14517
jd4yfrv9q_raw.fits	1000.5	2017-06-30	WFC	14517
jd4za0boq_raw.fits	1000.5	2017-07-03	WFC	14518
jd4za1c3q_raw.fits	1000.5	2017-07-03	WFC	14518
jd4za2ccq_raw.fits	1000.5	2017-07-03	WFC	14518
jd4za3cpq_raw.fits	1000.5	2017-07-03	WFC	14518
jd4za4jnq_raw.fits	1000.5	2017-07-05	WFC	14518
jd4za5l7q_raw.fits	1000.5	2017-07-05	WFC	14518
jd4za6lbq_raw.fits	1000.5	2017-07-05	WFC	14518
jd4za7lhq_raw.fits	1000.5	2017-07-05	WFC	14518
jd4za8q4q_raw.fits	1000.5	2017-07-07	WFC	14518
jd4za9qdq_raw.fits	1000.5	2017-07-07	WFC	14518
jd4zaaqmq_raw.fits	1000.5	2017-07-07	WFC	14518
jd4zabqyq_raw.fits	1000.5	2017-07-07	WFC	14518
jd4zacb2q_raw.fits	1000.5	2017-07-10	WFC	14518
jd4zadb9q_raw.fits	1000.5	2017-07-10	WFC	14518
jd4zaebrq_raw.fits	1000.5	2017-07-10	WFC	14518
jd4zafbzq_raw.fits	1000.5	2017-07-10	WFC	14518
jd4zagjvq_raw.fits	1000.5	2017-07-12	WFC	14518
jd4zahk4q_raw.fits	1000.5	2017-07-12	WFC	14518
jd4zaikbq_raw.fits	1000.5	2017-07-12	WFC	14518
jd4zajkoq_raw.fits	1000.5	2017-07-12	WFC	14518
jd4zaksfq_raw.fits	1000.5	2017-07-14	WFC	14518
jd4zalslq_raw.fits	1000.5	2017-07-14	WFC	14518
jd4zamsuq_raw.fits	1000.5	2017-07-14	WFC	14518
jd4zant2q_raw.fits	1000.5	2017-07-14	WFC	14518
jd4zaoahq_raw.fits	1000.5	2017-07-17	WFC	14518
jd4zapanq_raw.fits	1000.5	2017-07-17	WFC	14518
jd4zaqb4q_raw.fits	1000.5	2017-07-17	WFC	14518
jd4zarbiq_raw.fits	1000.5	2017-07-17	WFC	14518
jd4zasjhq_raw.fits	1000.5	2017-07-19	WFC	14518
jd4zatjnq_raw.fits	1000.5	2017-07-19	WFC	14518
jd4zaujzq_raw.fits	1000.5	2017-07-19	WFC	14518
jd4zavk9q_raw.fits	1000.5	2017-07-19	WFC	14518
jd4zawrzq_raw.fits	1000.5	2017-07-21	WFC	14518
jd4zaxs9q_raw.fits	1000.5	2017-07-21	WFC	14518

jd4zaysfq_raw.fits	1000.5	2017-07-21	WFC	14518
jd4zazt9q_raw.fits	1000.5	2017-07-21	WFC	14518
jd4zb0bqq_raw.fits	1000.5	2017-07-24	WFC	14518
jd4zb1c4q_raw.fits	1000.5	2017-07-24	WFC	14518
jd4zb2caq_raw.fits	1000.5	2017-07-24	WFC	14518
jd4zb3coq_raw.fits	1000.5	2017-07-24	WFC	14518

Table 4: List of the observations from the CCD Daily Monitor used in the characterization of the `ACSREJ` error treatment.